



Solid-state graphene-based supercapacitor with high-density energy storage using ionic liquid gel electrolyte: electrochemical properties and performance in storing solar electricity

Amr M. Obeidat^{1,2} · Vandna Luthra^{1,3} · A. C. Rastogi¹

Received: 21 December 2018 / Revised: 13 March 2019 / Accepted: 5 April 2019 / Published online: 18 April 2019
© Springer-Verlag GmbH Germany, part of Springer Nature 2019

Abstract

The electrochemical properties and high-density energy storage performance of graphene nano-platelet-based solid-state electrical double-layer supercapacitor device are reported. The graphene device is fabricated with electrolyte comprising of 1-butyl-3-methylimidazolium tetrafluoroborate (BMIMBF₄) room temperature ionic liquid and LiClO₄ dopant entrapped within polymer matrix formulated as a gel. The mesoporous graphene electrode was formed via dispersion in amorphous polyvinylidene (PVdF₂) host over flexible graphite sheets with minimal graphene layer (< 5-layer) stacking. Exploiting the abundance of charge ion species in the ionic liquid gel electrolyte and pervasive accesses to the graphene platelets via voids, high double-layer specific capacitance of 214 Fg⁻¹ was realized based on cyclic voltammetry data. Impedance studies show a low (0.79 Ω cm²) charge transfer resistance and a short Warburg range indicating highly diffusive ionic transport capability in the ionic liquid gel electrolyte. The Bode analysis showed high figure of merit for pulse power with 1145 ms response time and high-density (27 kWkg⁻¹) pulsed power capability of the graphene supercapacitor. The charge–discharge data show graphene supercapacitor by availing high (~ 2 V) stable potential window in ionic liquid electrolyte gel greatly boosted the energy density to 33.3 Whkg⁻¹ at power density 3 kWkg⁻¹ with minimal decrement to 24.7 Whkg⁻¹ at high ~ 3 Ag⁻¹ discharge current density. By integration with solar cells, direct storage of light-generated electricity and discharge behavior of ionic liquid electrolyte graphene supercapacitor is reported.

Introduction

Supercapacitors as electrical energy storage devices are most attractive for high-power applications. These have long cycle life and fast charge capability and require little maintenance. The energy storage in supercapacitors is basically by Faradaic redox mechanisms or by formation of an electrical double layer (EDL) much different from the battery mechanism which involves the chemical reactions rather than the physical process of ion absorption and accumulation [1]. The

supercapacitors which utilize the fast and reversible Faradaic surface and bulk redox reactions for the energy storage are mostly based on the transition metal (hydro) oxides [2] and electrically conducting polymers (ECP) [3]. The EDL supercapacitors on the other hand are based on high surface area activated carbon (AC) which provide vast interface for the accumulation of ions at the interface with the electrolyte. However, the access to electrolyte ions herein is only limited to a small fraction of the interface resulting in somewhat lower specific capacitance [4]. The electrodes based on the structured carbons like carbon nanotubes (CNT) have larger surface area and a distributed open pore structure accessible to the electrolyte ions [5], but are mostly used as composites with pseudocapacitive conducting polymers in order to boost the capacitance density. This results in a slower charge-discharge response and also affects the cyclic stability [6].

Graphene, comprising entirely of sp²-bonded carbon in the form of two dimensional layer, characterized by large surface area tunable up to theoretically predicted 2675 m² g⁻¹, high electrical conductivity, and mechanical flexibility have

✉ A. C. Rastogi
arastogi@binghamton.edu

¹ Department of Electrical and Computer Engineering, Center for Autonomous Solar Power, CASP, Binghamton University, State University of New York, Binghamton, NY 13902, USA

² Electrical Engineering Department, The Hashemite University, Zarqa 13115, Jordan

³ Department of Physics, Gargi College, New Delhi 110049, India

emerged as the potential EDL supercapacitor electrode material for the next generation energy storage devices with high-power capabilities [7–17]. In order to avail the maximum advantage of the graphene potential, the optimum choice of the electrolyte plays an important role. In particular, the built-up of the electrical double layer is dependent on the concentration and mobility of the participating ions and electrical conductivity of the electrolyte. Most past work on the graphene EDL supercapacitors has been reported on liquid organic electrolytes [7–13] which due to the limitation of < 2.5 V, chemically stable potential range and low electrical conductivity impede the realization-optimized capacity of graphene. Further, the inherent issues with liquid electrolytes which have adverse long-term effects on the supercapacitor functionalities are related to overcharging, corrosion, leakage-loss, short storage lifespan, and environment hazard.

In this context, the supercapacitors based on solid-state electrolytes have received extensive research impetus as these can be integrated with low-power electronics without any form factor concerns. Such supercapacitor devices assembled in the solid-state and flexible formats can be seamlessly integrated with the emergent flexible, wearable, and low-cost disposable electronics and therefore have much utility in highly adaptable energy storage [18–20] for high-power delivery. Combined with the solar cells [21], these can harvest, store, and condition the light-generated energy for diverse applications such as internet-activated electronics and wireless sensor networks [22, 23]. The liquid electrolyte-based supercapacitors on the other hand are assembled in the conventional cylindrical metal-encased forms using high safety encapsulation and thus are bulky. These are therefore less adaptive to integration of graphene supercapacitors in photovoltaic modules, fuel cells, or portable and flexible electronics applications.

The solid-state electrolytes are commonly based on cross-linked solid polymer or gel-polymer matrix which holds either neutral electrolyte salts or aqueous acidic or alkaline electrolyte phases [24]. The solid polymeric electrolytes have higher operating potential window spanning 3–4 V for better energy density, but have low conductivity in the range < 10^{-6} Scm^{-1} . Several studies are reported on activated carbon supercapacitors using solid-state electrolytes such as PVA-hypergrafted SiO_2 matrix with LiClO_4 with conductivity of 1.51×10^{-4} Scm^{-1} [25] and PVA- Na_2SO_4 hydrogel electrolyte [26] or PVA- LiClO_4 gel-electrolyte [27] with potential window of 1.8 V and 1.2 V, respectively. Similar studies in graphene have been aimed at flexible supercapacitors using cellulose-PVA- H_2SO_4 [28–30], micro-patterned interdigitated reduced graphene oxide electrodes using H_3PO_4 /PVA gel electrolyte [31] or the solution cast Nafion [32]. These aqueous gels with low (0–1 V) voltage range have low-energy-

power capability and suffer from water loss when used over wider temperature range critically affecting the performance.

Ionic liquids, with abundantly available charged ion species, chemically stable over practical temperature range, non-hazardous and having low vapor pressure offer a better option for EDL supercapacitors [33]. Further, most ionic liquids with wide stable potential range 1–4 V, [34] present an opportunity for achieving higher energy density beyond what is possible with organic electrolytes like acetonitrile which, due to toxicity and flammability, are less preferred. The graphene EDL supercapacitors have been reported using various ionic liquids in the solution form and a wide ranging specific energy and power values were demonstrated depending on the structural forms of graphene combined with the chemical nature of the ionic liquids [35–43].

The ionic liquids when entrapped within a polymer matrix of a gel polymer electrolyte could ameliorate the deficiencies of the conventional polymer electrolyte by combining each other's advantages into one solid-state ionic liquid-gel polymer electrolyte [44]. These ionic liquid gel polymer electrolytes used as film have high electrical conductivity ($\geq 10^{-4}$ S), electrochemical potential range up to 3.5 V, and broad practical temperature range. However, fewer studies have been reported on the assembly and performance of graphene EDL supercapacitors using the ionic liquids in the form of ionic liquid gel polymer electrolytes. These studies are focused on ionic liquids like 1-ethyl-3-methylimidazolium tetrafluoroborate (EMIMBF_4) as an electrolyte in a solid-state medium based on different polymer hosts, such as poly(acrylonitrile) [45], succinonitrile [46], polyvinylidene fluoride (PVdF_2) [44, 47–50], and graphene oxide-doped PVdF_2 [51]. In this work, we have investigated energy storage performance of graphene supercapacitor formed over flexible graphite sheet using 1-butyl-3-methylimidazolium tetrafluoroborate (BMIMBF_4) ionic liquid mixed with LiClO_4 dopant in the gel form using the composite of PVdF_2 and hexafluoropropylene (HFP) as amorphous polymer host. The amorphous state facilitates better ion dispersion and conduction of ions via void-like defects. The ionic liquid gel electrolyte also functions as a separator between the electrodes enabling highly simplified flat layer assembly of supercapacitors. This paper reports on the electrochemical energy storage performance of the LiClO_4 -doped BMIMBF_4 ionic liquid gel polymer electrolyte-based graphene supercapacitor. Further, by integration of such flat graphene supercapacitor device with the Si solar cell submodule, we have harvested the solar electricity and investigated the charging and discharging process in the solid-state graphene supercapacitor using ambient outdoor light. This paper reports the detailed results of investigations on the storage of solar cell-generated electricity.

Experimental

The graphene-based symmetrical supercapacitor device in the solid-state configuration was fabricated using identical graphene electrodes formed over flexible graphite sheets which also serve as current collectors. The graphene platelets with an average thickness of 8 nm, < 2 μm average lateral size, and having a large ~ 600 m² g⁻¹ surface area were used as the starting material. The graphene electrode was formed by slurry coating of a film using the doctor's blade method. The coated graphene electrodes were vacuum-dried overnight at ~ 100 °C before use in the fabrication of supercapacitor cell. The slurry comprised of graphene platelets was mixed with poly(vinylidene fluoride-hexafluoropropylene) (PVdF₂-HFP) polymer host in the 9:1 (w/w) ratio in n-methyl-2-pyrrolidone (NMP) solvent. The PVdF₂ component was kept in the amorphous state by the addition of HFP, and with high dielectric constant and low glass transition temperature, it serves as an ideal host for dispersion of graphene platelets. The scanning electron micrograph image of a graphene electrode in Fig. 1a shows uniform dispersion of graphene platelets thereby creating large proportion of mesoporosity with the average pore size of ~ 60 nm on the electrode. The solid electrolyte used in supercapacitor cell assembly was based on 1-butyl-3-methylimidazolium tetrafluoroborate (BMIMBF₄) room temperature ionic liquid formulated as a gel. The ionic liquid gel was formed with the host PVdF₂, Mw 400,000 polymer with BMIMBF₄ in the 20:80 weight ratio. Initially, the PVdF₂ was dissolved in acetone under stirring at 70 °C until a clear solution is obtained. To this solution, 0.1 M LiClO₄ was dissolved which acts as a dopant thus forming a viscous gel. The PVdF₂ with highly polar electronegative CF₂ groups is anodically stable electrochemical potential up to ~ 3.5 V. For fabrication of the supercapacitor device, the viscous ionic liquid gel polymer electrolyte was casted over each graphene electrodes and the acetone was allowed to evaporate in dry air. Later, the all solid-state graphene supercapacitor cells were assembled by placing the two gel-casted graphene electrodes over each other and pressed slightly thereby adhering and making close contact. Later, these were stored in an argon-filled glove box for ~ 2 h to ensure the complete evaporation of organic solvent before characterization. With the ionic liquid gel electrolyte also serving as a separator, such solid-state supercapacitor cells are compact, reliable, and free from leakage of the liquid component. The solid-state design simplifies the fabrication process, reduces the thickness of the device, and makes it compact for integration with various energy sources for storage such as solar cells without affecting the form factor.

Characterizations

The performance characteristics of the solid-state supercapacitor cells were evaluated by cyclic voltammetry (CV), Galvanostatic charge-discharge (GCD), and electrochemical impedance spectroscopy (EIS) techniques. The CV and GCD measurements were performed using the Solatron Electrochemical Interface (Model 1287). The cyclic voltammetry was carried out under various voltage ranges including -1.0 to 1.0, -1.5 to 1.5, and -2.0 to 2.0 V. The voltage was scanned from the anodic to cathode voltage direction at different rates between 5 and 100 mVs⁻¹ and respective currents *i_a* and *i_c* were recorded. Based on the electrochemically active electrode mass *M_{ac}*, the specific capacitance *C_{SV}* values was determined from the CV plots using the equation,

$$C_{SV} = \frac{|i_a(\max)| + |i_c(\max)|}{2 \cdot \nu_s \cdot M_{ac}} \quad (1)$$

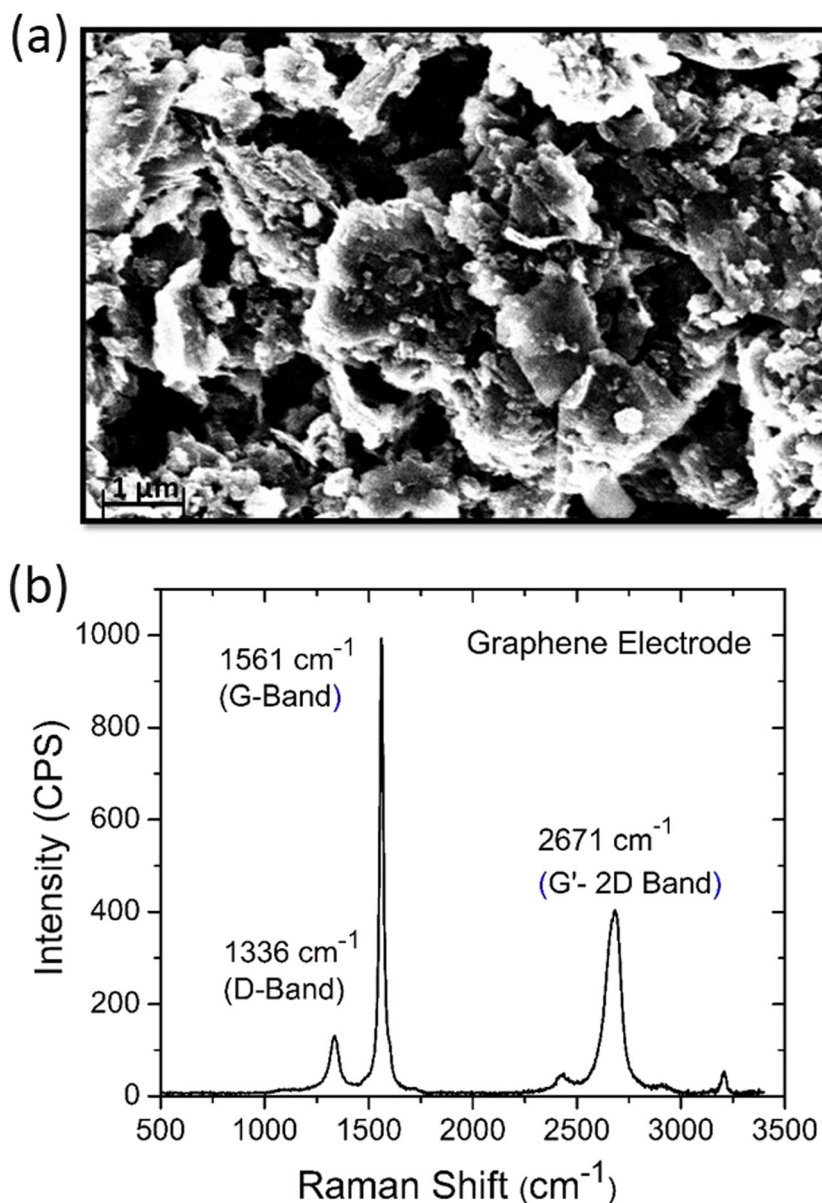
The Galvanostatic charge-discharge characteristics were measured in the same cell at constant load current densities in the range 0.1–3 Ag⁻¹ with the cell charging potentials, 0 to 1 V and 0 to 2 V. The specific gravimetric capacitance *C_{sd}*(Fg⁻¹) was evaluated from the slope of the discharge curve using the equation,

$$C_{sd} = \frac{2 I_L \cdot \Delta t_d}{m_{ac} \cdot \Delta V_d} \quad (2)$$

where *I_L* is the constant charging or load current, *m_{ac}* is single electrode mass, *Δt_d* is linear discharge time, and *ΔV_d* corresponding voltage variation after excluding the IR voltage drop. The ac impedance spectra were recorded in the frequency range of 0.01 Hz–100 kHz with ac signal amplitude of 10 mV using the Solatron gain-phase impedance analyzer (Model 1260). The impedance data provide frequency dependence of the real *Z_{Re}* and imaginary *Z_{Im}* impedances. The Nyquist plots between *Z_{Re}* and *Z_{Im}* based on the impedance data were simulated using the electrical equivalent circuit model representing the electrochemical and electrophysical properties of the graphene as an electrical double-layer capacitor using the Z-plot software (Scribner Associates) in order to obtain characteristic resistances and various contributing factors to the capacitance. The overall supercapacitor cell capacitance from the impedance study, *C_i*, is obtained by the relation *C_i* = (2π*fZ_{Im}*)⁻¹ where *f* is the signal frequency.

The morphology of the graphene platelet electrode was examined using a Zeiss Supra 55 field emission scanning electron microscope (FESEM). The Raman spectra of the graphene electrode were recorded in the 50–3500 cm⁻¹ range and resolution of 5 cm⁻¹ with a DXR Raman imaging microscope Thermo Scientific using 532-nm laser excitation.

Fig. 1 **a** SEM image of the graphene electrode synthesized by slurry coating. **b** Raman spectrum of corresponding graphene electrode



Results and discussion

Raman scattering spectrum of graphene platelet electrode

Raman scattering spectrum of graphene electrode was analyzed to understand the extent of graphene platelet stacking and any structural disorder resulting from the electrode assembly by slurry coating. A typical Raman spectrum of the graphene electrode coated over graphite sheet in Fig. 1b shows two main peaks at 1561 and 2671 cm⁻¹ designated as G and G'(2D) bands, respectively arising from in-plane and second-order overtone of a different in-plane C–C vibrational modes in the Sp² hybridized configuration arranged in a hexagonal network. As the G-band occurs at lower wavenumbers

relative to the single layer graphene at 1582 cm⁻¹, it is inferred that the platelets in the electrode are characterized by having graphene layer stacking [52]. Typically, the extent of graphene layer stacking reflects on the broadening and upward shift of the G'(2D) band [53]. As reported in [53], the G'(2D) band in graphene with 3–5 layers begins to show emergence of additional sub-components and beyond 5 layers the significant up shift in the 2700–2750 cm⁻¹ region. In our case, the G'(2D) Raman band in graphene electrode is a single peak and has a consistent match with the wavelength position with the graphene. It is inferred that in the graphene electrode, the layer stacking is < 5 layers. The somewhat lower intensity of the G'(2D) Raman band relative to pure graphene is due to the presence of (PVdF₂+HEP) host matrix in the electrode. The third major Raman peak at 1334 cm⁻¹ occurring at nearly half

the wavenumber position that of the 2D peak is due to the disorder-induced D-band. The intensity ratio $I_D/I_G = 0.133$ which being much smaller than 1 indicates that the disorder is not large [54]. The layer stacking of graphene, even though minimal in our case, is inevitable due to process steps involved in the preparation of electrode. This to an extent reduces inter-graphene pore spaces and to some extent restricts complete ion access to graphene platelets for electrical double-layer formation in utilizing the largest surface area possible with the graphene.

Cyclic voltammetry of graphene solid-state supercapacitor

The electrochemical capacitance property of the ionic liquid gel electrolyte-based symmetrical graphene supercapacitor was evaluated by cyclic voltammetry (CV) analysis carried out in the voltage ranges, -1.0 to 1.0 V, -1.5 to 1.5 V, and

-2.0 to 2.0 V, at variable scan rates of 5 – 100 mV s^{-1} and the results are shown in Figs. 2 (a), (b), and (c), respectively. The CV plots in all voltage ranges are highly symmetrical about the zero current axis and nearly rectangular in shape which testifies to highly capacitive behavior attributed to the electrified double-layer formed at the interface of graphene platelets and ionic liquid gel electrolyte. Due to significant π - π stacking interaction between the imidazolium and graphene, the $[\text{BMIM}]^+$ cations of the ionic liquid gel electrolyte have a higher tendency to attach and orientate parallel to the graphene platelets surface [55]. Such an interaction complements an expeditious formation of a homogeneous electrical double-layer encompassing the vast surface region of graphene platelets. The CV plots in the potential range ± 2 V (Fig. 2c) show a pair of broad reversible peaks in the near zero volt region both in the cathodic and anodic scans. These redox-like peaks, not evidenced in the CV plots at lower (<2 V) potentials (Figs. 2(c) and 4a), are attributed to the electro-reduction of

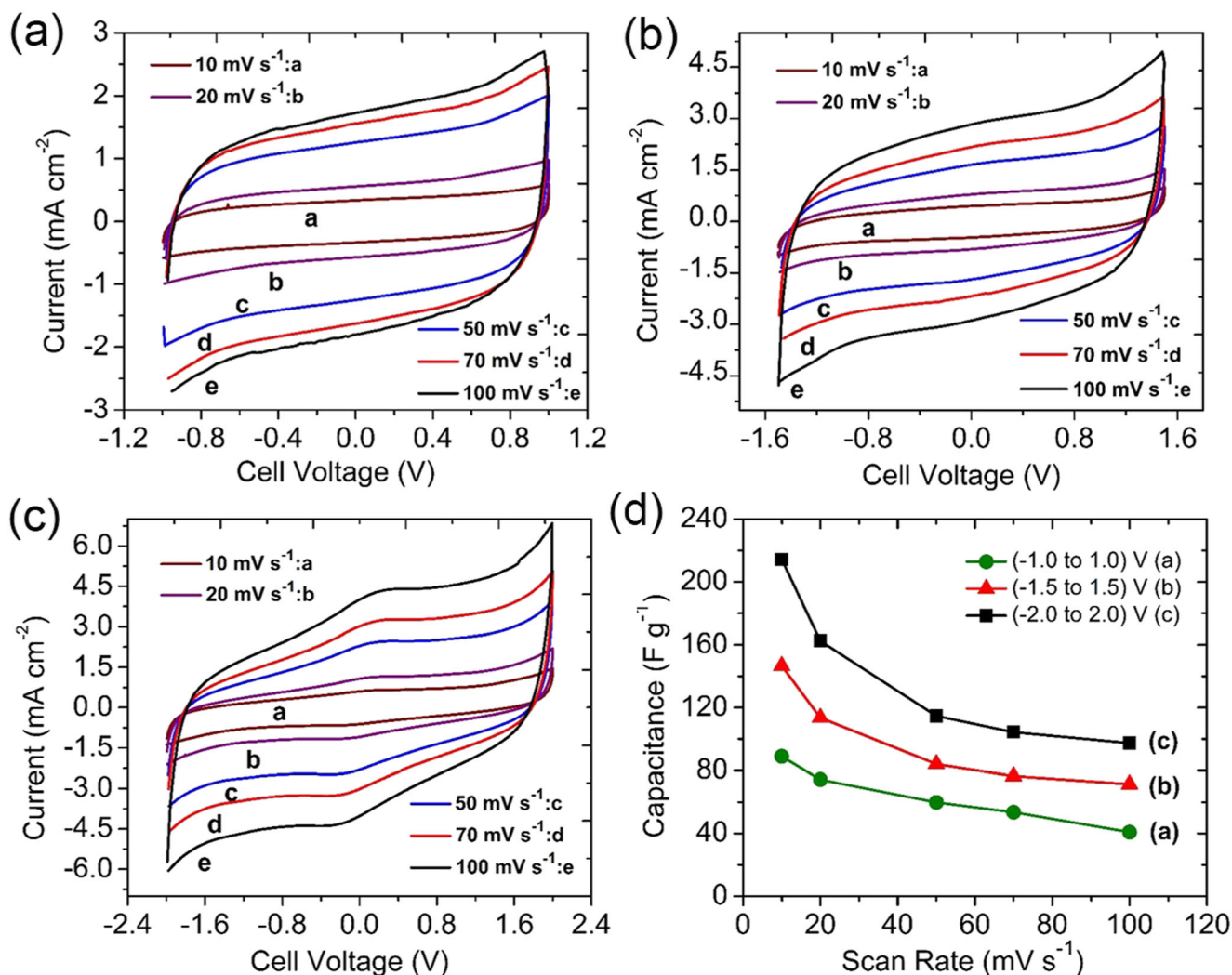


Fig. 2 CV curves of the graphene supercapacitor cell measured at scan rates of 5 – 100 mV s^{-1} in the voltage ranges (a) -1.0 to 1.0 V, (b) -1.5 to 1.5 V, and (c) -2.0 to 2.0 V. (d) Variation of specific capacitance as a function of the scan rate

adsorbed imidazolium [BMIM]⁺ cations over graphene platelets in the cathodic scans and electro-oxidation of BF₄⁻ anions in the anodic scans [56, 57]. These peaks hardly show any shift in potential with the scan rates which indicate faster kinetics of the ionic liquid redox activity. The pseudocapacitance due to redox reactions at the graphene platelets surface associated with the ionic liquid gel electrolyte add to the overall capacitance as evidenced from the increased currents in the CV plots. All CV plots irrespective of potential range show an almost instantaneous change in the current at the voltage corresponding to the peak voltage reversal as well as exhibit retention of the characteristic near rectangular shape of CV plots without distortion even as the voltage scan rate is increased to 100 mVs⁻¹. Both these observations suggest a faster ion kinetics which contributes to the improved capacitive property of graphene supercapacitor with the gel electrolyte. This is consistent with the inference that the capacitance originated due to the formation of a double-layer and ion adsorption at the vast graphene interface with the ionic liquid gel electrolyte.

Figures 3 (a) and (b) show the CV plots of the graphene supercapacitor cell measured within the negative voltage range -1.0 to 0 V, -1.0 to 0.2 V and -1.5 to 0 V, and -1.5 to 0.2 V at scan rates 10 and 50 mVs⁻¹, respectively. The CV curves for both scan rates are quasi-rectangular and show that the supercapacitor current is less dependent on the negative potential irrespective of the positive potential scanned. This is attributed to the adsorbed charges which increase with the increase in the potential thereby making current independent of the voltage which is a characteristic of the double-layer capacitance originating from surface aligned charges [58]. In contrast, when the supercapacitor voltage is scanned in negative to positive range and in the reverse, an increase in the cell

current is observed. This is shown by the CV plots in Fig. 4a which depict the effect of increasing voltages 1, 1.5, and 2 V scanned in both negative and positive directions at 20 mVs⁻¹ scan rates. In this case, with the reversal of the voltage, the realignment of the electric double layer over electrode involves diffusive transport of the ionic components BMIM⁺ and BF₄⁻ of the ionic liquid gel electrolyte. Similarly, as shown in CV plots in Fig. 2 (a)–(c), the current consistently increases with the increase in the scan rates in all voltage scans. Such observed increase in the current with the increase in the scan rates is due to diffusive ion charge transport not being synchronous with the electron transport. This is not unusual considering the differences in the charged state and size of the electrolyte ions and the electrons which results in the ions in motion lagging behind the electrons due to higher electronic mobility. This is also evident from Fig. 2 (d) showing a decrease in the specific capacitance values with the increasing scan rates for all three voltages. The specific capacitance of the supercapacitor was calculated from the CV plots using Eq. (1). Generally, the lowest scan rate-derived capacitance from the cyclic voltammetry plot is taken as the intrinsic specific capacitance of the supercapacitor material system. The highest specific capacitance of 214 Fg⁻¹ was realized at 10 mVs⁻¹ scan rate at 2 V and similarly 146 and 89 Fg⁻¹ at 1.5 and 1.0 V, respectively. The rate for capacitance decrease is faster for higher voltage scans. After an initial fast capacitance decline, the specific capacitance values nearly stabilize indicating that the graphene electrodes can be cycled at high scan rates up to 100 mVs⁻¹.

Figure 4b shows the increase in the specific capacitance with voltage calculated from the CV plots measured at a low (10 mVs⁻¹) scan rate which is taken as representative of the intrinsic capacitive value for energy storage ability of

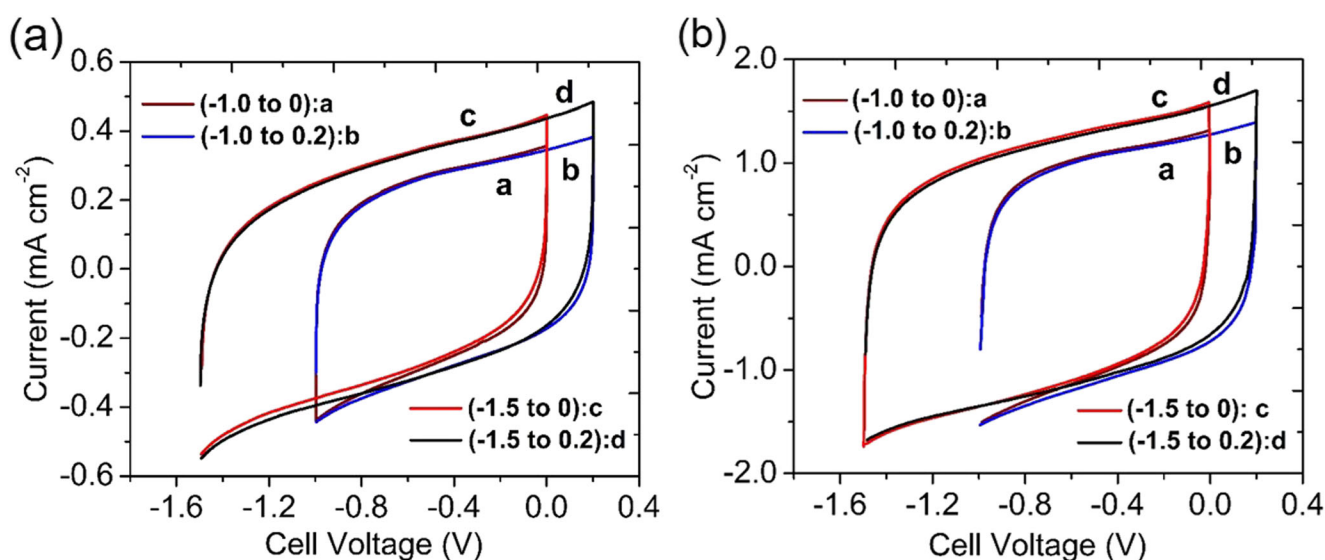


Fig. 3 CV plot of the graphene supercapacitor cell measured at scan rates of (A) 10 and (B) 50 mVs⁻¹. Negative voltage range are (a) -1.0 to 0 V, (b) -1.0 to 0.2 V, (c) -1.5 to 0 V, and (d) -1.5 to 0.2 V

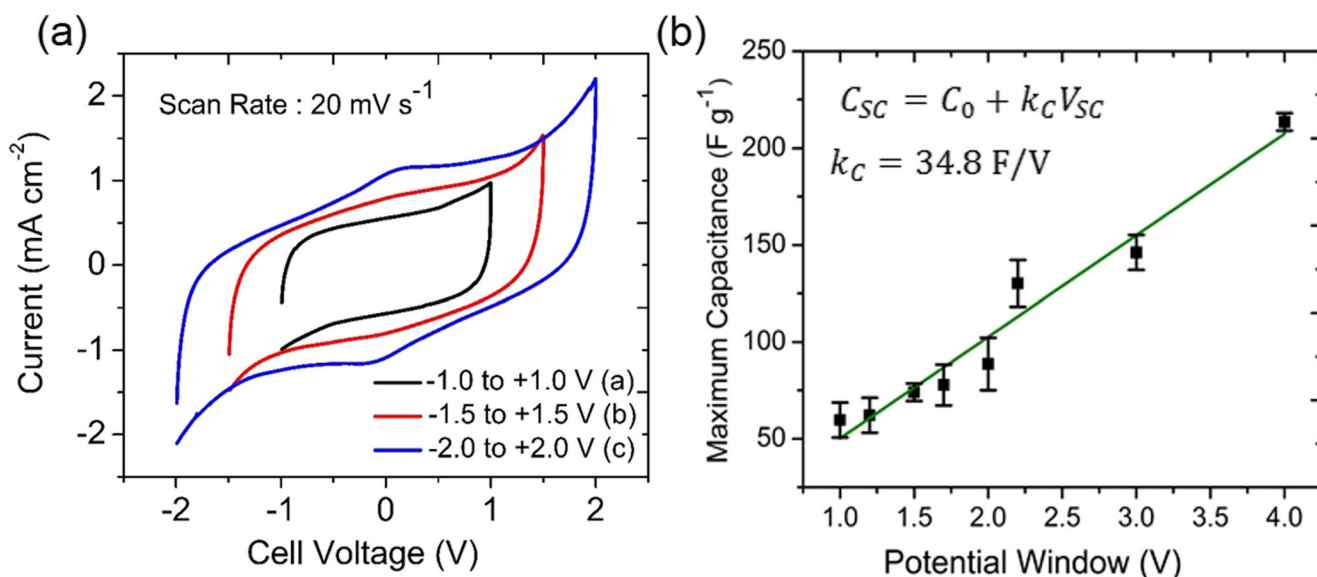


Fig. 4 **a** CV plots at increasing voltages 1, 1.5, and 2 V scanned in negative to positive voltage directions at 20 mVs^{-1} . **b** Increase in specific capacitance with voltage calculated from the CV plots measured at 10 mVs^{-1}

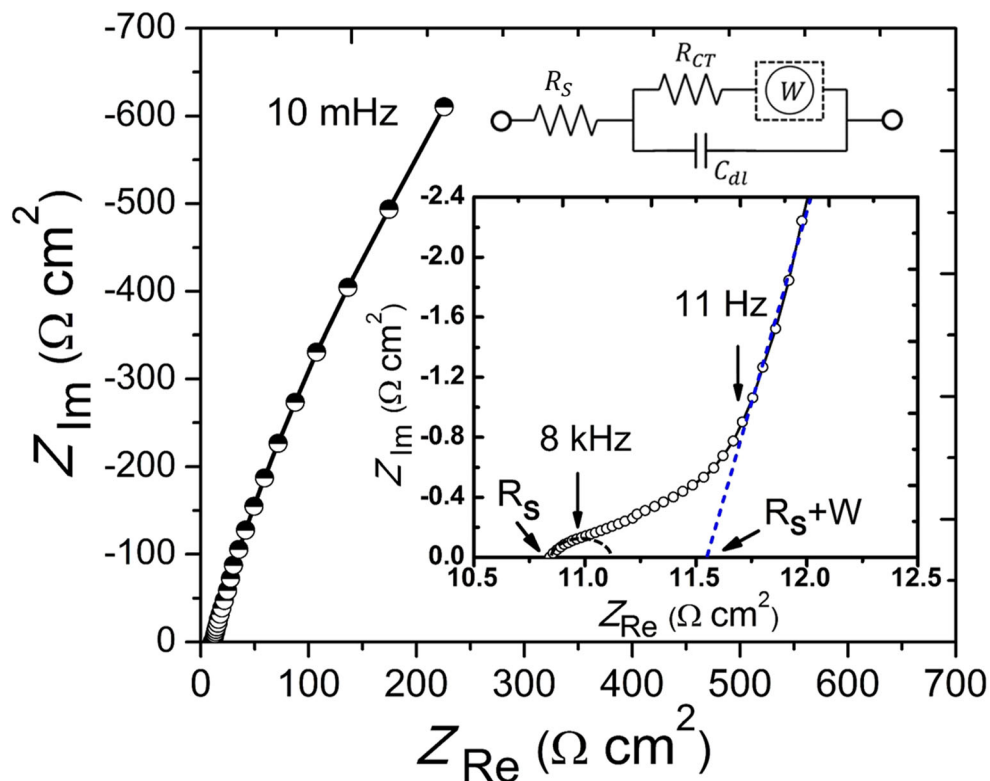
graphene supercapacitor device. The capacitance increases linearly with the charging voltage. Such voltage dependence capacitance being a typical attribute of the double-layer supercapacitors is consistent with the empirical relation $C_{SC} = C_0 + k_C \cdot V_{SC}$ where C_0 is the electrostatic capacitance, and the coefficient k_C defines the voltage dependency of the supercapacitor capacitance. A linear fit of the measured capacitance with voltage shows intercept C_0 is nearly zero and k_C value 34.8 F/V . This implies that in ionic liquid gel electrolyte graphene supercapacitor, the entire capacitance is contributed by the electrical double layer at the interface of the graphene platelets. Thus, the ionic liquid gel electrolyte-based graphene supercapacitor by virtue of high voltage operation is capable of showing improvement in the energy density performance, compared with the aqueous or solid polymeric electrolyte-based supercapacitors which typically have a lower breakdown voltage.

Electrochemical impedance spectra of graphene supercapacitor

A typical impedance behavior of the supercapacitor cell analyzed in the form of a Nyquist plot (Fig. 5) depicts the dependency of the real Z_{Re} and imaginary Z_{Im} impedances over a wide $10 \text{ mHz} - 100 \text{ kHz}$ frequency range. The graphene electrode supercapacitor in conjunction with the ionic liquid gel polymer electrolyte shows capacitive properties as reflected by the steep rising behavior of the Z_{Im} impedance plot in the low-frequency region. The high and mid-frequency impedance region is shown in the expanded form in the inset of Fig. 5. This region basically characterizes the bulk resistance properties of electrolyte, R_S , and the interfacial charge transfer resistance R_{CT} of the supercapacitor system. The experimental

impedance data of the Nyquist plot in the high and mid-frequency domain are fitted to a semicircle. Its origin is attributed to the frequency response of the double-layer capacitance (C_{dl}) in parallel with the charge transfer resistance (R_{CT}) at the electrode-electrolyte interface as shown by the electrical equivalent circuit in Fig. 5. The Z_{Re} axis cut-off at $R_S = 10.83 \Omega \text{ cm}^2$ quantifies the internal resistances with contributions from uncompensated electrolyte-electrode resistance. The mid-frequency intercept of the semicircle yields $R_S + R_{CT}$ from which R_{CT} value is derived to be $0.79 \Omega \text{ cm}^2$. The low R_{CT} value, considering the solid-state design of the supercapacitor with ionic liquid gel electrolyte, is significant as it represents proximity of ions with the graphene platelets without the encumbrance of exchange of charges across the electrical double layer. Beyond the semicircle cut-off on the real Z_{Re} axis lies a linear region of 45° angularity spread over $200 - 40 \text{ Hz}$ signifying the Warburg impedance (W). The short Warburg range indicates that the diffusive transport of electrolyte ions and their access to the graphene platelets in the electrodes are not a major limitation. A near vertical increase in the imaginary impedance Z_{Im} with only a little shift on the Z_{Re} axis following the Warburg region denotes the capacitive behavior of the supercapacitor which extends over a wide frequency domain beginning with the knee frequency at the end of the Warburg region down to the lowest frequency of 0.01 Hz . The knee frequency at 11 Hz is consistent with the high-rate capability of the ionic liquid gel electrolyte-based graphene supercapacitor. The cut-off of the linear extension of the low frequency impedance beyond the knee frequency on the real Z_{Re} axis gives a value $R_S + R_\Omega$ where R_Ω signifies $1/3$ of the ionic resistance. The calculated R_Ω value of $3.86 \Omega \text{ cm}^2$ from the impedance plot (Inset Fig. 5) essentially arises from the resistance encountered by ions from distributed RC

Fig. 5 Nyquist plot of the graphene supercapacitor measured in (10 mHz–100 kHz) frequency range. Inset shows impedance plots in expanded frequency region 100 kHz–12 Hz and the electrical equivalent circuit



network of the pores in the graphene electrode. The specific electrode capacitance, C_{SI} based on Z_{Im} value at 0.01 Hz, is calculated as 78.6 Fg^{-1} . The extent to which the cation and anion species of the ionic liquid gel electrolyte are able to access the graphene platelets in the electrode was qualitatively evaluated from the frequency dependence of the real capacitance. The ion access essentially determines the degree of formation of the electrical double layer which is important for the rate capability of the supercapacitor as well as its storage energy density. The supercapacitor is modeled as an electrical equivalent circuit comprising of a parallel combination of a capacitor and resistor connected to a series resistance as shown in Fig 5. The capacitance C_{sc} is defined in terms of the real capacitance, C' , and imaginary capacitance, C'' , by a complex relation [59],

$$C_{sc}(\omega) = C'(\omega) - jC''(\omega) \quad (3)$$

The real capacitance C' is effectively involved in the actual delivery of the stored capacitive energy to the load and it is determined from the impedance data using the relation [59],

$$C'(\omega) = \frac{-Z_{Im}(\omega)}{\omega|Z(\omega)|^2} \quad (4)$$

where Z and Z_{Im} are the complex and imaginary impedances measured at angular frequency ω .

Figure 6a presents the frequency variation of real capacitance calculated from the measured impedances depicted in the Nyquist plots. The near zero plateau over a broader mid-frequency to high frequency indicates the resistive response of the supercapacitor and the zero capacitance implies minimal contact of the electrolyte with the graphene platelets. The capacitive behavior of supercapacitor is observed in the rapid increase in $C'(\omega)$ as the frequency decreases below 6 Hz. In the transition regime extending down to ~ 40 mHz, the real capacitance C' has a near linear rise representing the parallel RC response. This region reflective of properties of the electrode-electrolyte interface indicates that graphene platelets have a reasonable access to the BMIM^+ and BF_4^- component ions of the ionic liquid gel electrolyte. A decrease in the slope of the linear transition region below 40 mHz suggests an approach towards a pure capacitance response. The observed sluggish change $C'(\omega)$ and a near maximum value at ~ 10 mHz indicate in-depth permeation of the ions in the interior and surrounding the highly dispersed graphene platelets in the electrode structure. The maximum capacitance value shows a saturating response over a shorter frequency range. This suggests that only a near complete charged state of the supercapacitor electrodes has possibly been attained. This is attributed to the limitation of the diffusive ion transport usually seen in porous electrodes. The pulsed power performance of the ionic liquid gel electrolyte-based graphene supercapacitor was evaluated from the characteristic response of the real Z_{Re} and imaginary impedances Z_{Im} [60, 61]. The response depicted in Fig. 6b

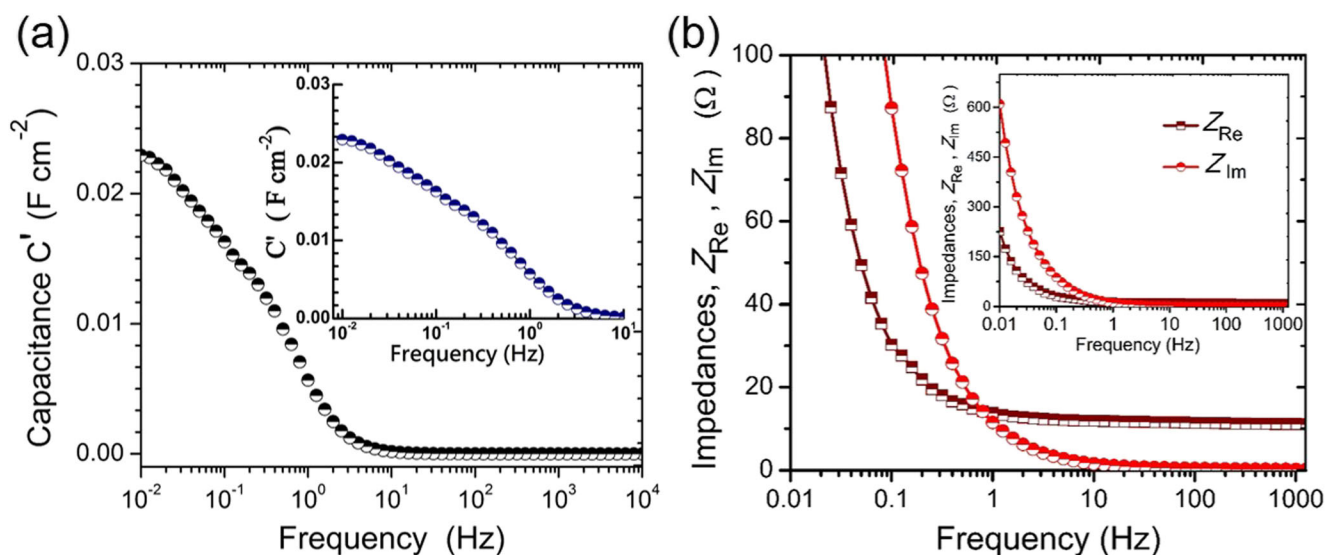


Fig. 6 **a** Frequency variation of real capacitance calculated from the measured impedances. **b** Response identifying the specific frequency f_0 having equal magnitude of both Z_{Re} and Z_{Im}

identifies a specific frequency f_0 of 874 mHz at which both Z_{Re} and Z_{Im} are equal in magnitude. This yields the characteristic pulse power response time $\tau_0 = (f_0)^{-1}$ of 1145 ms. This shows that the ionic liquid gel-based graphene EDLC is suitable for the most high pulsed power applications. The available energy density E_{d0} was calculated from the equation $E_{d0} = 0.5C_0V^2/M_{SC}$ as 8.59 Whkg^{-1} . Here, C_0 is evaluated from Z_{Im} value at f_0 as $C_0 = (2\pi f_0 Z_{Im})^{-1}$; M_{SC} is the combined electroactive mass of both supercapacitor electrodes and V is the rated supercapacitor voltage. The figure of merit for the assessment of the pulsed power performance is basically the available pulsed power density P_{d0} based on E_{d0}/τ_0 . The calculated $P_{d0} = 27 \text{ kWkg}^{-1}$ indicates high pulsed power capability of ionic liquid gel electrolyte graphene supercapacitor.

Galvanic charge-discharge behavior of graphene supercapacitor

The energy-power performance of the ionic liquid gel electrolyte graphene supercapacitor device was evaluated by studying the Galvanic charge-discharge (GCD) characteristics at various load currents I_L in the range 0.12 to 3.0 Ag^{-1} for charging voltages 1 and 2 V . The typical GCD curves for 1 V shown in Fig. 7 (a) and (b) and for 2 V in Fig. 8a are linear across the entire charging and discharging times for both voltages reaffirming the capacitive nature arising from the electrical double layer in the graphene supercapacitor device. The specific gravimetric capacitance C_{sd} (Fg^{-1}) was evaluated from the slope of the discharge curve using the equation $C_{sd} = 2I_L \cdot \Delta t/m_{ac}\Delta V$ (Eq. (2)) where I_L is the constant charging or load current and m_{ac} is single electrode mass. The discharge time Δt and corresponding capacitor voltage change ΔV were determined by excluding the sudden voltage

drop due to the equivalent series resistance (ESR). The ESR reflective of the internal cell resistance has contribution from ionic mobility in the electrolyte and electronic resistance of active graphene electrode and contacts. The specific gravimetric capacitance of graphene with ionic liquid gel electrolyte derived from the discharge curves is 112 Fg^{-1} at 1 V and 119 Fg^{-1} at 2 V at a current density of 0.15 and 0.13 Ag^{-1} , respectively.

The graphene electrodes as reported in the past have shown a diverse range of specific capacitance values which are mostly based on either aqueous or organic liquid electrolytes with strong dependence on various preparatory methods and different chemical activation processes. Chemically modified graphene supercapacitor in KOH and acetonitrile showed specific discharge capacitance of 95 and 128 Fg^{-1} , respectively at 20 mA [62], and 117 Fg^{-1} in aqueous H_2SO_4 electrolyte using the thermally exfoliated graphene [63]. Similarly, graphene synthesized from graphene oxide by microwave expansion showed specific capacitance of 191 Fg^{-1} in KOH [64] and by thermal reduction in polycarbonate yielded 122 Fg^{-1} in organic electrolytes [65]. Besides these SO_4 and OH anion-based liquid electrolytes, by employing EMIMBF₄ ionic liquid solution, gravimetric discharge capacitance of 154.1 Fg^{-1} was shown in supercapacitors using the curved graphene sheets [36] and 116.1 Fg^{-1} in supercapacitor having hierarchical graphene/activated carbon composite aerogel electrode [41]. In the present study, the gravimetric capacitance realized in graphene supercapacitor in the solid state design using the BMIMBF₄ ionic liquid gel electrolyte is generally comparable with the liquid electrolyte values with the exception to recently reported somewhat higher 306 Fg^{-1} capacitance density in the hydrogen annealed graphene supercapacitors [38]. Our results show that the ion access to the vast interiors of the

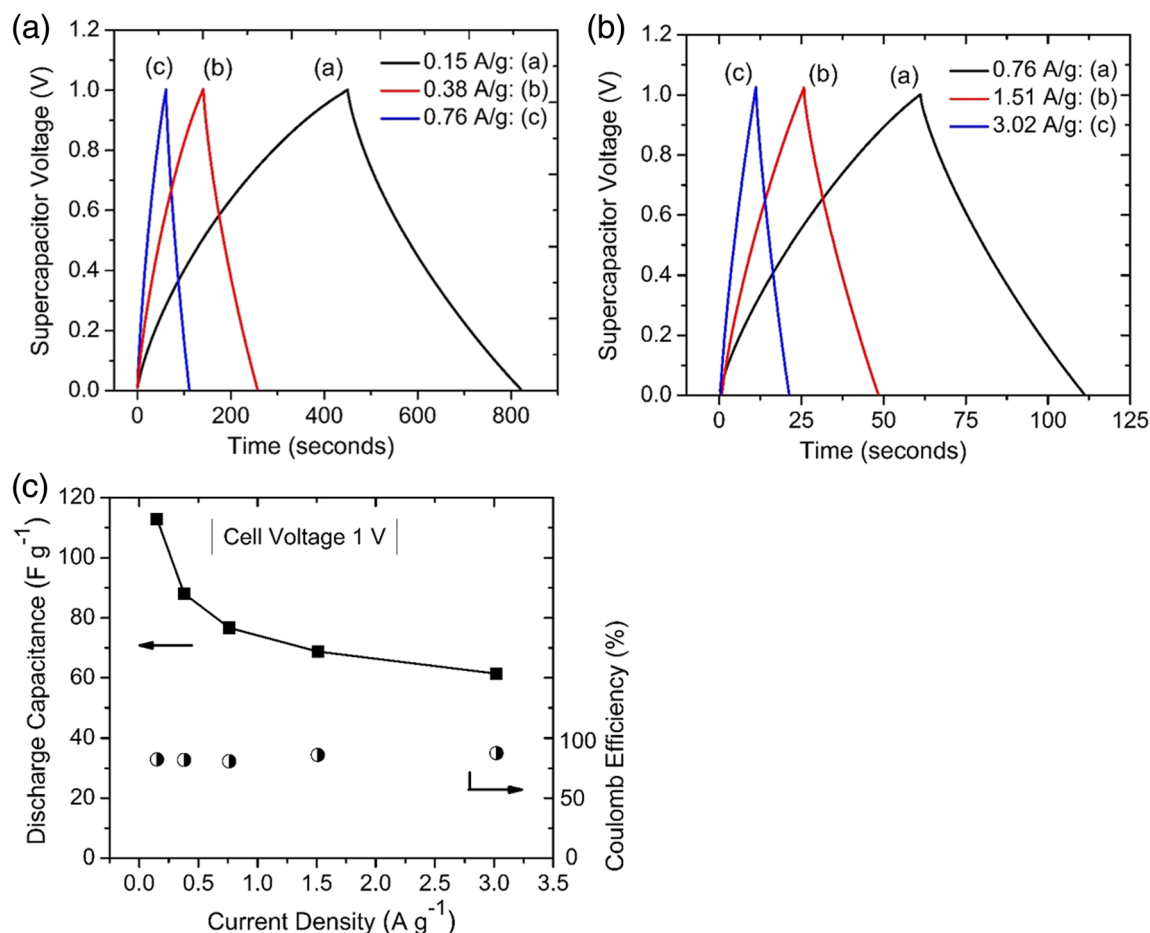


Fig. 7 Charge-discharge characteristics for charging voltage 1 V at various load currents in the range of (a) 0.15 to 0.76 A g⁻¹ and (b) 0.76 to 3.02 A g⁻¹. (c) Variation in the discharge capacitance of the graphene

supercapacitor cell as a function of current density. Variation in Coulombic efficiency as a function of current density is also shown

graphene electrode and attaining reasonably high ion mobility or high conductivity have not been a limitation with ionic liquid gel electrolyte. In the past, graphene supercapacitor devices based on solid polymer or gel polymeric electrolytes have typically shown capacitance density in the 80–118 F g⁻¹ range [28]. Further improvement in the gravimetric capacitance at 1 A g⁻¹ were only made possible with the exceptional structural or chemical modification of graphene which led to open pore graphene structure such as by laser reduction (204 F g⁻¹) [66], hydrogel graphene with 3-dimensional microstructure (186 F g⁻¹) [30], or by ionic liquid functionalization of graphene (167 F g⁻¹) [29]. The electrolyte phase in these supercapacitors was embedded in polymer hydrogel PVA-H₂SO₄ or PVA-H₃PO₄.

Figure 7 (c) shows the nonlinear dependence of the specific capacitance of graphene supercapacitor on the load current density. Typically, the specific capacitance decreases by ~28% as current density increases by four times under low (< 0.5 A g⁻¹) current regime. The specific capacitance derived from low constant current charging and discharging reflects the intrinsic charge storage capability of the ionic liquid gel

electrolyte graphene supercapacitor. The capacitance decrease is due to the difference in the electrolyte ions kinetics with the relatively faster electronic process. However, in the higher current range (> 0.5 A g⁻¹), the specific capacitance nearly levels out between 75 and 60 F g⁻¹, decreasing only by 19% as current density is increased by six times. This indicates that ionic liquid gel electrolyte graphene supercapacitor can deliver higher current without much detriment of the energy storage capability. The graphene supercapacitor charged to higher voltage of 2 V shows nominally higher specific capacitance of 119 F g⁻¹ than the 112 F g⁻¹ realized at 1 V at almost identical charging current. As shown in Fig. 8b, herein, the decrease in specific capacitance is much smaller and levels of at a higher range 95–87 F g⁻¹ with the increase in the charging current density from 0.5 to 2.9 A g⁻¹. The Coulomb efficiency of the ionic liquid gel electrolyte graphene supercapacitor was obtained from the ratio of discharge to charge time in the CD plots in Figs. 7 (a) and (b) and 8a. As the results in Figs. 7 (c) and 8b show, the Coulomb efficiency is in the range of 82–87% and 94–97% for graphene supercapacitor charged to 1 and 2 V, respectively. The Coulomb efficiency is basically a

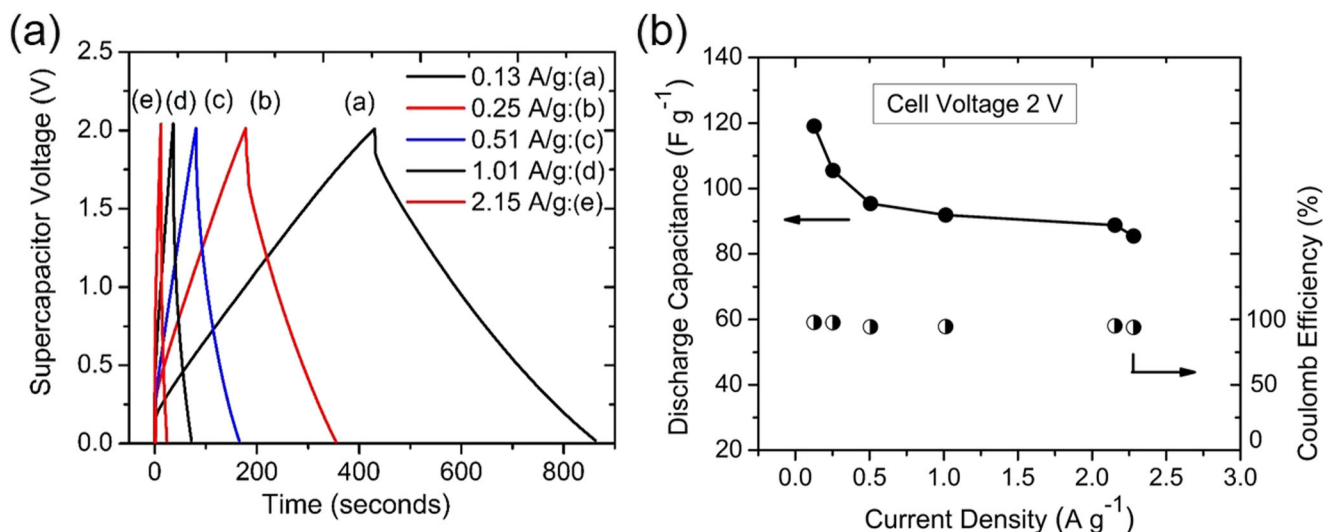


Fig. 8 **a** Charge-discharge characteristics for charging voltage 2 V at various load currents in the range of 0.13 to 2.15 A g⁻¹. **b** Variation of discharge capacitance and Coulombic efficiency as a function of the current density at cell voltage 2 V

measure of the loss of stored charge at delivery to a load on account of leakage of charges or the redistribution ions at the electrode-electrolyte interface. The high Coulomb efficiency for the supercapacitor cells under study is comparable with most aqueous electrolyte graphene supercapacitors.

Energy-power performance of graphene supercapacitor

The parametric relationship of the storage energy density and related power density provides a greater insight of the device functional aspects of the ionic liquid gel electrolyte graphene supercapacitor cells. The gravimetric specific energy (Whkg⁻¹) was calculated using the combined active electrode mass M_{ac} at different load current densities when supercapacitor was charged to voltage V_{sc} of 1 and 2 V using the expression,

$$E_d = \frac{1}{2M_{ac}} \cdot C_{sd} \cdot V_{sc}^2 \quad (5)$$

The corresponding maximum gravimetric specific power (kWkg⁻¹) at matched impedance was obtained from the expression [67, 68],

$$P_d = \frac{V_{sc}^2}{4M_{ac} \cdot ESR} \quad (6)$$

where ESR is the equivalent series resistance of the supercapacitor cell and was calculated as $ESR = V_{drop}/2I_L$, where V_{drop} is the sudden voltage drop at the start of the discharge curve. The ESR is a measure of internal cell resistance and the low ESR values are attributed to high electrical conductance of ionic liquid gel electrolyte combined with the low graphene electrode resistances.

The specific energy and power parameters of the ionic liquid gel electrolyte graphene supercapacitors charged to 1 and 2 V are shown in the Ragone plots in the upper and lower panels of Fig. 9, respectively. The supercapacitor charged to 1 V shows a specific energy of 7.7 Whkg⁻¹ at corresponding specific power of 16.8 kWkg⁻¹. The specific energy value realized here is comparable or better than those reported on graphene supercapacitors at 1 V but shows much higher specific power indicating high rate capability of the device configured with ionic liquid gel electrolyte. In the past, with liquid electrolytes specific energy of 2.93 Whkg⁻¹ (Na₂SO₄) in spray-formed graphene [69], 4.7 Whkg⁻¹ (KOH, 135 Fg⁻¹) in chemically modified graphene device [52], 9.2 Whkg⁻¹ in vacuum exfoliated graphene device [70], and much improved 28.5 Whkg⁻¹ (KOH) in hydrazine reduced graphene oxide [7] have been reported.

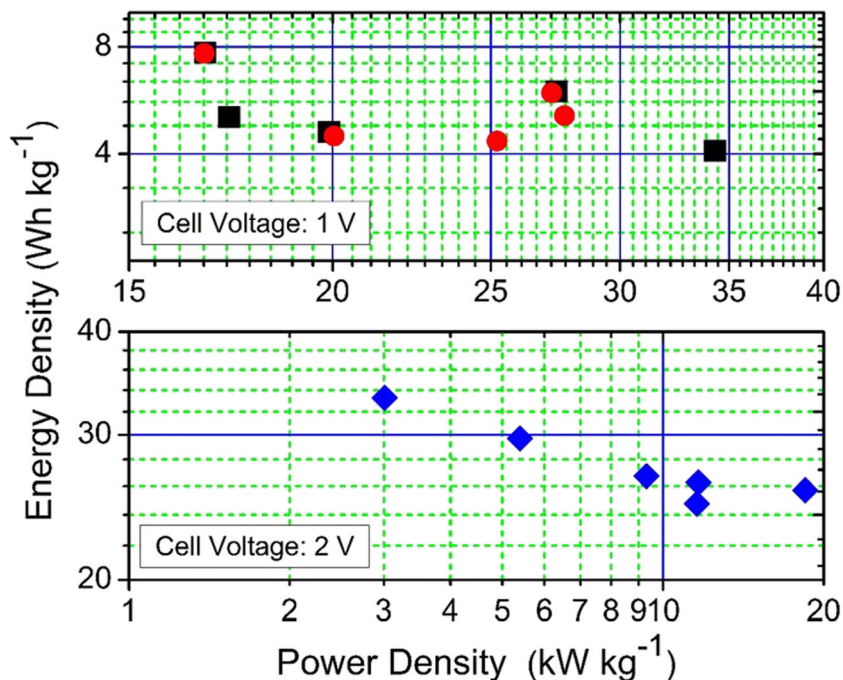
At 2 V in our case, the graphene supercapacitor with the ionic liquid gel electrolyte shows higher specific energy values but corresponding specific power values are lower relative to the similar supercapacitor device charged to 1 V. A high specific energy of 33.3 Whkg⁻¹ at specific power of 3 kWkg⁻¹ was observed as shown in Fig. 9. In the literature, high (2–3.5 V) voltage graphene supercapacitor device has been reported in either ionic liquid solutions or in the organic liquid electrolytes. For example, using EMIMBF₄ ionic liquid electrolyte solution, Wang et al. [41] reported a specific energy of 34.6 Whkg⁻¹ (3 V, 0.63 kWkg⁻¹), Rao et al. 31.9 Whkg⁻¹ (3.5 V) [63], Liu et al. 85.6 Whkg⁻¹ (3.5 V, 0.8 kWkg⁻¹) [36], and recently Yang et al. 148.7 Whkg⁻¹ (3 V, 30.9 kWkg⁻¹) [38]. In organic or aqueous electrolytes, the corresponding specific energy values at cell potentials 1.8–3 V were 28.3 Whkg⁻¹ [66], 31.39 Whkg⁻¹ [38], and 28.5 Whkg⁻¹ [7] which are relatively lower to those obtained in ionic liquid electrolytes.

It is evident that the graphene supercapacitor in the solid state configuration with ionic liquid gel polymer electrolyte being reported here has the specific energy values comparable with liquid electrolyte assembled supercapacitors. Apparently, the swiftness of the ion transport and pervasive ion access for built-up of the electrical double layer at the graphene platelet interface with ionic liquid gel polymer electrolyte is achieved at a level similar to that which is characteristically possible with the liquid electrolytes. Previously, diverse specific energy values for solid-state graphene supercapacitors based on various polymer electrolytes were reported [29, 30, 45–47]. For example, using PVA-H₂SO₄ hydrogel electrolyte—specific energy of 19.7 Whkg⁻¹ [29] and 6.5 Whkg⁻¹ [30], and as in the present case using different ionic liquids embedded polymer host electrolytes, specific energy of 8.2 Whkg⁻¹ [46], 7.4 Whkg⁻¹ (1 V) [47], and 30.51 Whkg⁻¹ (3 V) [45] have been reported. It is worth mentioning that ionic liquid-polymer electrolytes used in structured carbon-based supercapacitors have shown much smaller specific energy values in the range 13–20 Whkg⁻¹ [71, 72]. Improvement in specific energy to 92 Wh kg⁻¹ was reported using the EMEIMBF₄ gel electrolyte by functionalization of graphene [49] and 75 Wh kg⁻¹ by forming graphene as hierarchical nanocomposite with polyaniline-derived carbon [50] in supercapacitor cells charged to 3.5 V. The graphene supercapacitor device in the present study tested at 2 V cell potential has shown comparably or higher specific energy and specific power values than those reported at

3–3.5 V which indicates that the BMIMBF₄-PVdF₂ ionic liquid gel electrolyte with LiClO₄ dopant has better compatibility with the graphene. The charging of double layer in ionic liquid has strong dependence on the distribution of strongly interacting cations and anions. Consequently, the structure of electrical double layer and thus performance of supercapacitor could be affected by the charge and size of ions [33, 73]. More specifically, the role of constituent ions of the ionic liquid electrolyte in graphene double-layer capacitor has been discussed in earlier reports [74, 75].

The variation of the specific energy with increasing specific power as shown in Fig. 9 reminisces the behavior of an electrical double-layer supercapacitor power device exemplified by the tendency towards the reduction in specific energy as specific power increases when higher load currents are applied. In the ionic liquid gel electrolyte graphene supercapacitor charged to 1 V, the decrement in energy density is not as significant at the corresponding increase in the power density. The E_d values are in the range 10 ± 2 Whkg⁻¹ as the power density increases from 17 to 35 kWkg⁻¹ which suggests high power functionality of the ionic liquid gel electrolyte graphene supercapacitor. In the case of supercapacitor device charged to 2 V, the specific energy decrement is slightly aggravated. From a base value of 33.3 Whkg⁻¹ at 3 kWkg⁻¹, the specific energy is levels of at ~ 24.7 Whkg⁻¹ for enhancement in the specific power to 20 kWkg⁻¹. These data show that graphene supercapacitor in solid state platform with BMIMBF₄ ionic liquid gel electrolyte with PVdF₂ as

Fig. 9 Variation in specific energy with increasing specific power of the graphene supercapacitor at cell voltages 1 V (upper) and 2 V (lower) panel



highly ionic polymer host could be useful in high power applications without much penalty on the energy storage capability.

Long-term cyclic stability

The stability of graphene platelet supercapacitor was evaluated by sequential charge-discharge (CD) for 8000 cycles at 1.1 Ag^{-1} current density charged to 1 and 2 V (Fig. 10). In the case of graphene, supercapacitor charged to 2 V, after an initial capacitance fading by 10% until ~ 1600 CD cycle and a gradual decline of 5% thereafter for about 4000 CD cycles nearly 100% retention is observed. When the supercapacitor was charge to 1 V, the capacitance is nearly invariant for the first 1600 CD cycles, records a steady decline by $\sim 10\%$ for the next 2400 CD cycles, and exhibits a stable performance further on recording overall 10% decline over 8000 CD cycles. The equivalent series resistance (ESR) value of the graphene platelet supercapacitor shows an increase with the cycling (Fig. 10a). The ESR is caused by electrolyte ion conductivity and electronic resistance of graphene electrode. Since the increase in the ESR is consistent with the corresponding decline in the specific capacitance suggests this could be a factor in cyclic stability of the graphene supercapacitor. The overall cyclic performance of the graphene platelet supercapacitor at 1 V is within the normal parameters and no significant degradation in the graphene platelet electrode is observed. To understand the relatively higher rate of initial capacitance decline in supercapacitor charged at 2 V, Raman spectrum of graphene electrode after disassembling the supercapacitor device was examined for possible structural modification after the cyclic test. The graphene

Raman spectra (Fig. 10b) in the post-cycled state show an increase in the intensity ratio of the disordered induced D to G band from I_D/I_G 0.13 to 0.39 and a reduction the intensity of the G'-2D band with no change in the peak positions. Since the G band reflects ordered Sp^2 domains and D to the defected graphitic domains, the increase in the intensity ratio suggests increase in the disorder in the graphene electrode after cycling [50]. It is anticipated that intrusion-extraction of $[\text{BMIM}]^+[\text{BF}_4]^-$ ions may result in the increases spacing between the adjacent graphene layers [76], while the reduction in the G'-2D band also supports the disorder, with no apparent change in its wavenumber position or any observed broadening suggests no change in the layer stacking in the post-cycled graphene electrode [77] (Fig. 10b).

Harvesting solar cell-generated electricity using graphene supercapacitors

The utility of ionic liquid gel electrolyte-based graphene supercapacitor cell in the storage of solar photovoltaic electrical energy was investigated. Due to the planar thin layer configuration, such graphene supercapacitors can be integrated underneath the solar cells without any form-factor concerns. Such energy harvesting system can be of potential application in portable low power electronics or wearable electronics. Figure 11a shows the electrical test circuit used to study the energy storage performance when the supercapacitor was directly charged by a Si solar cell sub-module exposed to light. The switches S1 and S2 were alternatively closed and opened for charging (storage) and discharging (power delivery) into a resistive load. A blocking diode prevents supercapacitor from discharging into the characteristic resistances of the Si solar

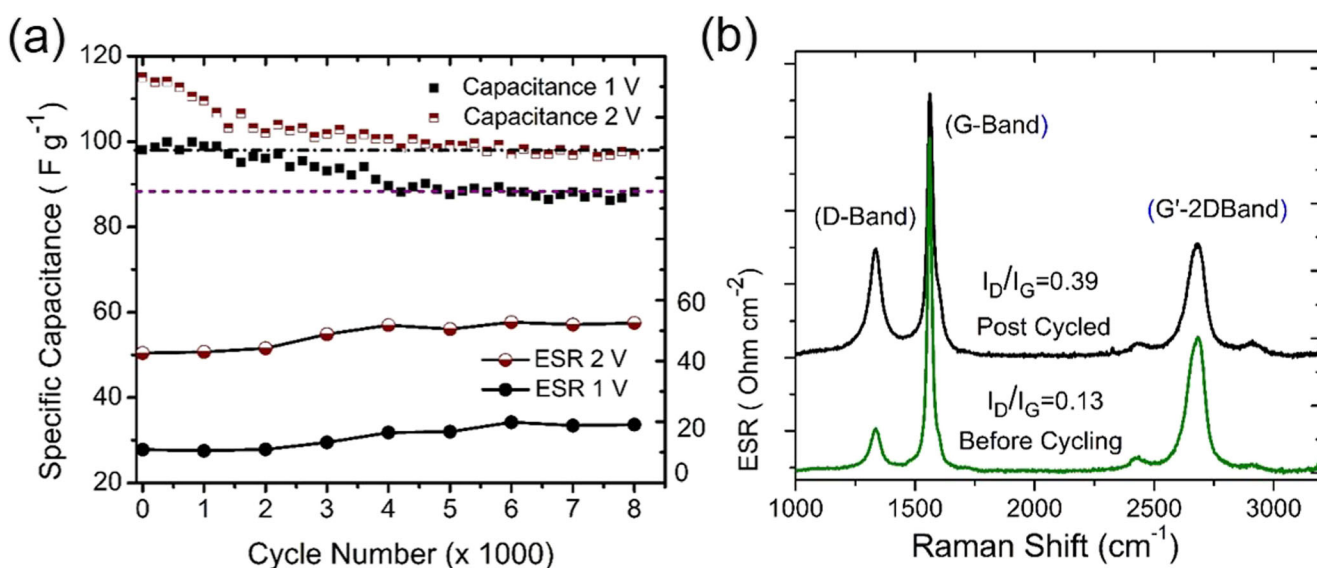


Fig. 10 **a** Cyclic stability of graphene platelet supercapacitor with ionic liquid gel electrolyte charged to 1 and 2 V at 1.1 Ag^{-1} and corresponding change in ESR for 8000 charge-discharge cycles. **b** Raman spectrum of graphene electrode before and after cyclic test

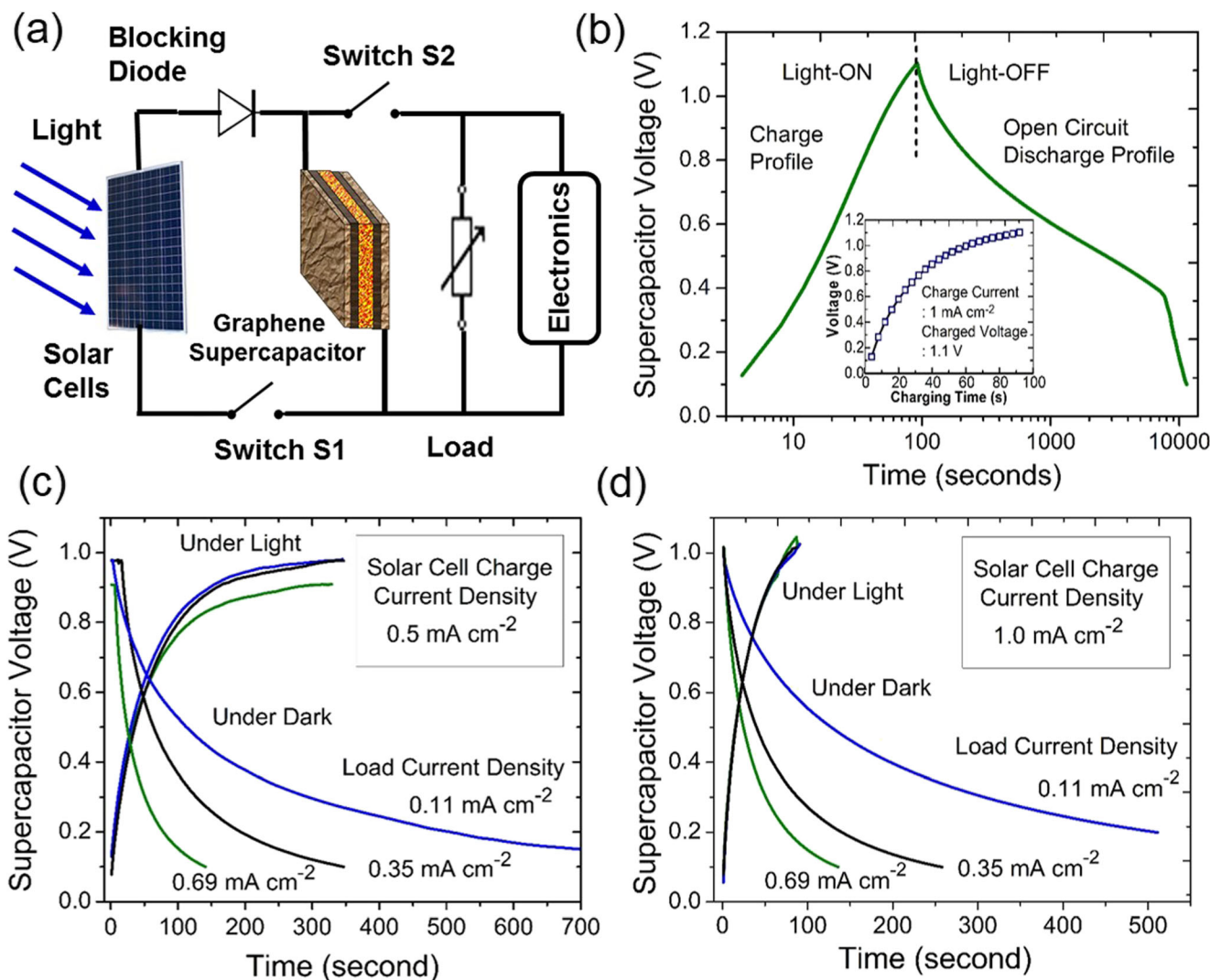


Fig. 11 **a** Electrical test circuit used to study energy storage performance. **b** CD characteristics of the ionic liquid gel electrolyte graphene supercapacitor charged by solar cell to 1.1 V. CD profile by charging

the supercapacitor to 1 V by light-generated solar cell under current densities of 0.5 mAcm⁻² (c) and 1.0 mAcm⁻² (d)

cell module. The charging and discharging characteristics of supercapacitor were evaluated by monitoring the voltage profile with time using computer-controlled digital multimeter Agilent 34401A. Figure 11b shows the charging and charge retention (open circuit) characteristics of the ionic liquid gel electrolyte graphene supercapacitor charged by the solar cell to 1.1 V when light radiation of 70 mWcm⁻² intensity was incident on the solar cell submodule. The expanded charging profile is shown in the inset. The graphene supercapacitor charges rapidly to 1.1 V within 90 s when light over solar cell is turned on. The discharge curve under open circuit condition is obtained after the light incident over solar cell is turned off and the switch S1 is kept open. The self-discharge characteristic shows that it takes ~8000 s (2 h 13 min) for voltage to fall to 0.4 V. Over the initial monitored period of 1100 s (~18 min), the cell voltage falls to 0.6 V but thereafter, significantly slowly to 0.4 V for nearly 6900 s (1 h 54 min). The

complete self-discharge occurs in 11460 s (3 h 11 min). The extended energy storage period shows that the ionic liquid gel electrolyte graphene supercapacitor holds considerable potential for self-powered electronics by storing solar electricity when integrated with solar cells. Figure 11 (c) and (d) show the CD profile by charging the supercapacitor to 1 V by light-generated solar cell current density of 0.5 and 1.0 mA cm⁻², respectively and discharge curves in dark at various load resistances. The discharge rate is nonlinear and discharge times are dependent on the load resistance. With charging time of 318 s to 1.0 V at 0.5 mAcm⁻² current from solar cell, the discharge times of 700, 350, and 150 s were observed for load resistance 10, 3.2, and 1.6 kΩ, respectively corresponding to currents 0.11, 0.35, and 0.69 mAcm⁻². When the solar cell charging current was 1 mAcm⁻², it took about 90 s to charge and the discharge times are 520, 260, and 145 s at corresponding current density values of 0.11, 0.35, and 0.69 mAcm⁻²,

respectively. The longer discharge current times for graphene supercapacitor charged at low solar cell current are due to spatial alignment of the electrical double layer at the ionic liquid gel electrolyte graphene interface due to slower ion kinetic relative to the electronic process when charged at higher currents. The initial current of 0.11, 0.35, and 0.69 mAcm⁻² drawn from a supercapacitor for these arbitrarily chosen resistances is considerably higher for most low-power portable electronics. Further, at slow charging using ambient light on solar cell and using low load currents, the ionic liquid gel electrolyte graphene supercapacitor is capable of providing even extending powering times.

Conclusions

The graphene nano-platelets-based solid-state electrical double-layer supercapacitor energy storage device is fabricated using the 1-butyl-3-methylimidazolium tetrafluoroborate (BMIMBF₄) room temperature ionic liquid with 0.1 M LiClO₄ dopant formulated as gel polymer electrolyte. The graphene electrode formed via dispersion in amorphous PVdF₂+HFP host has large proportion of mesoporosity and as Raman studies show has minimal (<5 layer) restacking. The cyclic voltammetry studies show double-layer specific capacitance scales with cell voltage leading to high specific capacitance of 214 Fg⁻¹ at 2 V compared with previously reported values and are attributed to the abundance of charge ion species in ionic liquid gel electrolyte and pervasive access to graphene platelets via voids. Impedance data simulated using an electrical equivalent circuit shows much lower (0.79 Ωcm²) charge transfer resistance, a short Warburg range signifying high diffusive ionic transport, and a knee frequency value of 11 Hz consistent with high rate capability in ionic liquid gel electrolyte. The near saturation behavior of real capacitance at lower (~10 mHz) frequency further confirms in-depth permeation of ions in the interior regions surrounding the graphene platelets. From Bode analysis, the figure of merit with characteristic response time of 1145 ms and capability for high pulse power density of 27 kWkg⁻¹ has been shown. The charge–discharge data show that the graphene supercapacitor by availing high (~2 V) stable potential in ionic liquid gel electrolyte greatly boosted the energy density to 33.3 Whkg⁻¹ at power density of 3 kWkg⁻¹ with minimal decrement to 24.7 Whkg⁻¹ at high ~3 Ag⁻¹ discharge current density. Facilitated by flat solid-state cell assembly, by the integration of graphene supercapacitor device with solar cells, direct storage of light-generated electricity is demonstrated which is highly relevant to emergent flexible, wearable, and low-cost disposable electronics for highly adaptable energy storage. The graphene supercapacitor in the solid-state design showed long-term charge holding capability of up to 3 h 11 min self-discharge (50%) times and various charge release

rates dependent on the load current density. The observed discharge rates of 520, 260, and 145 s at current density of 0.11, 0.35, and 0.69 mAcm⁻², respectively are adequate to power most emergent portable electronics.

Funding information This research was financially supported by the National Science Foundation, under Award Number 1318202, “Partnership for Innovation in Electrochemical Energy Storage” which is gratefully acknowledged. VL thanks the University Grant Commission (UGC) India for the Raman visiting fellowship. The authors also acknowledge the grant ADLG-181 from Analytical and Diagnostics Laboratory (ADL), a part of Center of Excellence in Small Scale Integration and Packaging at Binghamton University

References

- Kötz R, Carlen M (2000) Principles and applications of electrochemical capacitors. *Electrochim Acta* 45:2483–2498
- Wang G, Zhang L, Zhang J (2012) A review of electrode materials for electrochemical supercapacitors. *Chem Soc Rev* 41:797–828
- Snook GA, Kao P, Best AS (2011) Conducting-polymer-based supercapacitor devices and electrode. *J Power Sources* 196:1–12
- Zhang LL, Zhao XS (2009) Carbon-based materials as supercapacitor electrodes. *Chem Soc Rev* 38:2520–2253
- Candelaria SL, Shao Y, Zhou W, Li X, Xiao J, Zhang J-G, Wang Y, Liu J, Li J, Cao G (2012) Nanostructured carbon for energy storage and conversion. *Nano Energy* 1:195–220
- Yan XB, Chen JT, Yang J, Xue QJ, Miele P (2010) Fabrication of free-standing electrochemically active and biocompatible graphene oxide-polyaniline and graphene-polyaniline hybrid papers. *ACS Appl Mater Interfaces* 2:2521–2529
- Wang Y, Shi Z, Huang Y, Ma Y, Wang C, Chen M, Chen Y (2009) Supercapacitor devices based on graphene materials. *J Phys Chem C* 113:13103–13107
- Zhu Y, Murali S, Cai W, Li X, Suk JW, Potts JR, Ruoff RS (2010) Graphene and graphene oxide: synthesis, properties, and applications. *Adv Mater* 22:3906–3924
- Huang X, Zeng Z, Fan Z, Liu J, Zhang H (2012) Graphene-based electrodes. *Adv Mater* 24:5979–6004
- Pumera M (2011) Graphene-based nanomaterials for energy storage. *Energy Environ Sci* 4:668–674
- Deng W, Ji X, Gomez-Mingot M, Lu F, Chen Q, Banks CE (2012) Graphene electrochemical supercapacitors: the influence of oxygen functional groups. *Chem Commun* 48:2770–2772
- Xu Z, Li Z, Holt CMB, Tan X, Wang H, Amirkhiz BS, Tyler S, Mitlin D (2012) Electrochemical supercapacitor electrodes from sponge-like graphene nanoarchitectures with ultrahigh power density. *J Phys Chem Lett* 3:2928–2933
- Liu W, Yan X, Lang J, Pu J, Xue Q (2013) Supercapacitors based on graphene nanosheets using different non-aqueous electrolytes. *New J Chem* 37:2186–2195
- Shao Q, Tang J, Lin Y, Li J, Qin F, Zhang K, Yuan J, Qin L (2015) Ionic liquid modified graphene for supercapacitors with high rate capability. *Electrochim Acta* 176:1441–1446
- Kim TY, Lee HW, Stroller M, Dreyer DR, Bielawski CW, Ruoff RS, Suh KS (2011) High performance supercapacitor based on poly(ionic liquid)-modified graphene electrodes. *ACS Nano* 5:436–442
- Ke Q, Wang J (2016) Graphene-based materials for supercapacitor electrodes—a review. *J Mater* 2:37–54
- Raccichini R, Varzi A, Passerini S, Scrosati B (2015) The role of graphene for electrochemical energy storage. *Nat Mater* 14:271–279

18. Jost K, Stenger D, Perez CR, McDonough JK, Lian K, Gogotsi Y, Dion G (2013) Knitted and screen printed carbon-fiber supercapacitors for applications in wearable electronic. *Energy Environ Sci* 6:2698–2705
19. Hu L, Pasta M, Mantia FL, Cui L, Jeong S, Deshaze HD, Choi JW, Han SM, Cui Y (2010) Stretchable, porous, and conductive energy textiles. *Nano Lett* 10:708–714
20. Wang K, Zou W, Quan B, Yu A, Wu H, Jiang P, Wei Z (2011) An all-solid-state flexible micro-supercapacitor on a chip. *Adv Energy Mater* 1:1068–1072
21. Zhang Z, Chen X, Chen P, Guan G, Qiu L, Lin H, Yang Z, Bai W, Luo Y, Peng H (2014) Integrated polymer solar cell and electrochemical supercapacitor in a flexible and stable fiber format. *Adv Mater* 26:466–470
22. Zhan Y, Mei Y, Zheng L (2014) Materials capability and device performance in flexible electronics for the internet of things. *J Mater Chem C* 2:1220–1232
23. Somov A, Ho CC, Passerone R, Evans JW, Wright PK (2012) Towards extending sensor node lifetime with printed supercapacitors. *Wireless Sensor Networks; Proceedings of the 9th European Conference (EWSN 2012), Trento, Italy: 212–227*
24. Choudhury NA, Sampath S, Shukla AK (2009) Hydrogel-polymer electrolytes for electrochemical capacitors: an overview. *Energy Environ Sci* 2:55–67
25. Hu XL, Hou GM, Zhang MQ, Rong MZ, Ruan WH, Giannelis EP (2012) New nanocomposite polymer electrolyte based on poly(vinyl alcohol) incorporating hypergrafted nano-silica. *J Mater Chem* 22:18961–18967
26. Batisse N, Raymundo-Piñero EA (2017) Self-standing hydrogel neutral electrolyte for high voltage and safe flexible supercapacitors. *J Power Sources* 348:168–174
27. Chodankar NR, Dubal DP, Lokhande AC, Lokhande CD (2015) Ionically conducting PVA-LiClO₄ gel electrolyte for high performance flexible solid state supercapacitors. *J Colloid Interface Sci* 460:370–376
28. Weng Z, Su Y, Wang D, Li F, Du J, Cheng H (2011) Graphene-cellulose paper flexible supercapacitors. *Adv Energy Mater* 1:917–922
29. Choi BG, Chang S, Kang H, Park CP, Kim HJ, Hong WH, Lee S, Huh YS (2012) High performance of a solid-state flexible asymmetric supercapacitor based on graphene films. *Nanoscale* 4:4983–4988
30. Xu Y, Lin Z, Huang X, Liu Y, Huang Y, Duan X (2013) Flexible solid-state supercapacitors based on three-dimensional graphene hydrogel films. *ACS Nano* 7:4042–4049
31. Niu Z, Zhang L, Liu L, Zhu B, Dong H, Chen X (2013) All-solid-state flexible ultrathin micro-supercapacitors based on graphene. *Adv Mater* 25:4035–4042
32. Choi BG, Hong J, Hong WH, Hammond PT, Park H (2011) Facilitated ion transport in all-solid-state flexible supercapacitors. *ACS Nano* 5:7205–7213
33. Eftekhari A (2017) Supercapacitors utilizing ionic liquids. *Energy Storage Materials* 9:47–69
34. Wei D, Ng TW (2009) Application of novel room temperature ionic liquids in flexible supercapacitors. *Electrochem Commun* 11:1996–1999
35. Lei Z, Liu Z, Wang H, Sun X, Lu L, Zhao XS (2013) A high-energy-density supercapacitor with graphene-CMK-5 as the electrode and ionic liquid as the electrolyte. *J Mater Chem A*:2313–2321
36. Liu C, Yu Z, Neff D, Zhamu A, Jang BZ (2010) Graphene-based supercapacitor with an ultrahigh energy density. *Nano Lett* 10:4863–4868
37. Yang C, Huang P, Luo X, Wang C, Li C, Wu Y, Chang J (2015) Holey graphene nanosheets with surface functional groups as high-performance supercapacitors in ionic-liquid electrolyte. *ChemSusChem* 8:1779–1786
38. Yang H, Kannappan S, Pandian AS, Jang J, Lee YS, Lu W (2017) Graphene supercapacitor with both high power and energy density. *Nanotechnology* 28:445401–445411
39. Kim J, Kim S (2014) Preparation and electrochemical property of ionic liquid-attached graphene nanosheets for an application of supercapacitor electrode. *Electrochim Acta* 119:11–15
40. Chen Y, Zhang X, Zhang D, Ma Y (2012) High power density of graphene-based supercapacitors in ionic liquid electrolytes. *Mater Lett* 68:475–477
41. Wang X, Lu C, Peng H, Zhang X, Wang Z, Wang G (2016) Efficiently dense hierarchical graphene based aerogel electrode for supercapacitors. *J Power Sources* 324:188–198
42. Kim J, Kim S (2014) Surface-modified reduced graphene oxide electrodes for capacitors by ionic liquids and their electrochemical properties. *Appl Surf Sci* 295:31–37
43. Lin Z, Taberna P, Simon P (2016) Graphene-based supercapacitors using eutectic ionic liquid mixture electrolyte. *Electrochim Acta* 206:446–451
44. Obeidat AM, Rastogi AC (2018) Electrochemical energy storage performance of asymmetric PEDOT and graphene electrode-based supercapacitors using ionic liquid gel electrolyte. *J Appl Electrochem* 48:747–764
45. Tamilarasan P, Ramaprabhu S (2013) Graphene based all-solid-state supercapacitors with ionic liquid incorporated polyacrylonitrile electrolyte. *Energy* 51:37–81
46. Singh MK, Suleman M, Kumar Y, Hashmi SA (2015) A novel configuration of electrical double layer capacitor with plastic crystal based gel polymer electrolyte and graphene nano-platelets as electrodes: a high rate performance. *Energy* 80:465–473
47. Pandey GP, Rastogi AC (2012) Graphene-based all-solid-state supercapacitor with ionic liquid gel polymer electrolyte. *MRS Proc* 1440. <https://doi.org/10.1557/opl.2012.1279>
48. Obeidat AM, Rastogi AC (2016) Graphene and poly(3, 4-ethylenedioxythiophene) (PEDOT) based hybrid supercapacitors with ionic liquid gel electrolyte in solid state design and their electrochemical performance in storage of photovoltaic generated electricity. *MRS Advances* 1(53):3565–3571
49. Ujjain SK, Sahu V, Sharma RK, Singh G (2015) High performance all solid state, flexible supercapacitor based on ionic liquid functionalized graphene. *Electrochim Acta* 157:245–251
50. Feng L, Wang K, Zhang X, Sun X, Li C, Ge X, Ma Y (2018) Flexible solid-state supercapacitors with enhanced performance from hierarchically graphene nanocomposite electrodes and ionic liquid incorporated gel polymer electrolyte. *Adv Funct Mater* 28:1704463–1704469
51. Yang X, Zhang L, Zhang F, Zhang T, Huang Y, Chen Y (2014) A high-performance all-solid-state supercapacitor with graphene-doped carbon material electrodes and a graphene oxide-doped ion gel electrolyte. *Carbon* 72:381–386
52. Gupta A, Chen G, Joshi P, Tadigadapa S, Eklund PC (2006) Raman scattering from high-frequency phonons in supported n-graphene layer films. *Nano Lett* 6:2667–2673
53. Ferrari AC (2007) Raman spectroscopy of graphene and graphite: disorder, electron-phonon coupling, doping and nondiabetic effects. *Solid State Commun* 143:47–57
54. Childres I, Jauregui LA, Park W, Cao H, Chen YP (2013) Raman spectroscopy of graphene and related materials. *New developments in photon and materials research*, ed. J. I. Jang, Nova Science Publishers
55. Vijayakumar M, Schwenzer B, Shutthanandan V, Hu J, Liu J, Aksay IA (2014) Elucidating graphene-ionic liquid interfacial region: a combined experimental and computational study. *Nano Energy* 3:152–158

56. Xiao L, Johnson KE (2003) Electrochemistry of 1-butyl-3-methyl-1*H*-imidazolium tetrafluoroborate ionic liquid. *J Electrochem Soc* 150:E307–E311
57. Zheng J, Moganty SS, Goonetilleke PC, Baltus RE, Roy D (2011) A comparative study of the electrochemical characteristics of [Emim+][BF₄⁻] and [Bmim+][BF₄⁻] ionic liquids at the surfaces of carbon nanotube and glassy carbon electrodes. *J Phys Chem C* 115:7527–7537
58. Conway BE (1999) *Electrochemical supercapacitors*. Springer, Boston, MA
59. Taberna PL, Simon P, Fauvarque JF (2003) Electrochemical characteristics and impedance spectroscopy studies of carbon-carbon supercapacitors. *J Electrochem Soc* 150:A 292–A 300
60. Miller JR, In: Proceedings of the eighth international seminar on double layer capacitors and similar energy storage devices, Deerfield Beach, Florida, December 1998.
61. Lufitano F, Staiti P, Minutoli M (2003) Evaluation of nafion based double layer capacitors by electrochemical impedance spectroscopy. *J Power Sources* 124:314–320
62. Stoller MD, Park S, Zhu Y, An J, Ruoff RS (2008) Graphene-based ultracapacitors. *Nano Lett* 8:3498–3502
63. Vivekchand SR, Chandra SR, Subrahmanyam KS, Govindaraj A, Rao CNR (2008) Graphene-based electrochemical supercapacitors. *J Chem Sci* 120:9–13
64. Zhu Y, Murali S, Stoller MD, Velamakanni A, Piner RD, Ruoff RS (2010) Microwave assisted exfoliation and reduction of graphite oxide for ultracapacitors. *Carbon* 48:2118–2122
65. Zhu Y, Stoller MD, Cai W, Velamakanni A, Piner ARD, Chen D, Ruoff RS (2010) Exfoliation of graphite oxide in propylene carbonate and thermal reduction of the resulting graphene oxide platelets. *ACS Nano* 4:1227–1233
66. El-Kady MF, Strong V, Dubin S, Kaner RB (2012) Laser Scribing of High-Performance and Flexible Graphene-based electrochemical capacitors. *Science* 335:1326–1330
67. Burke A (2000) Ultracapacitors: why, how, and where is the technology. *J Power Sources* 91:37–50
68. Zhu Y, Murali S, Stoller MD, Ganesh KJ, Cai W, Ferreira PJ, Pirkle A, Wallace RM, Cychosz KA, Thommes M, Su D, Stach EA, Ruoff RS (2011) Carbon-based supercapacitors produced by activation of graphene. *Science* 332(6037):1537–1541
69. Beidagh M, Wang Z, Gu L, Wang C (2012) Electrostatic spray deposition of graphene nanoplatelets for high-power thin-film supercapacitor electrodes. *J Solid State Electrochem* 16:3341–3348
70. Lv W, Tang DM, He YB, You CH, Shi ZQ, Chen XC, Chen CM, Hou PX, Liu C, Yang QH (2009) Low-temperature exfoliated graphenes: vacuum-promoted exfoliation and electrochemical energy storage. *ACS Nano* 3:3730–3736
71. Lu W, Henry K, Turchi C, Pellegrino J (2008) Incorporating ionic liquid electrolytes into polymer gels for solid-state ultracapacitors. *J Electrochem Soc* 155:A361–A367
72. Pandey GP, Kumar Y, Hashmi SA (2010) Ionic liquid incorporated polymer electrolytes for supercapacitor application. *Indian J Chem* 49A:743–751
73. Sillars FB, Fletcher SI, Mirzaeian M, Hall PJ (2012) Variation of electrochemical capacitor performance with room temperature ionic liquid electrolyte viscosity and ion size. *Phys Chem Chem Phys* 14: 6094–6100
74. Huang P, Luo X, Peng Y, Pu N, Ger M, Yang C, Wu T, Chang J (2015) Ionic liquid electrolytes with various constituent ions for graphene-based supercapacitors. *Electrochim Acta* 161:371–377
75. Liu W, Yan X, Lang J, Xue Q (2011) Electrochemical behavior of graphene nanosheets in alkylimidazolium tetrafluoroborate ionic liquid electrolytes: influences of organic solvents and the alkyl chains. *J Mater Chem* 21:13205–13212
76. Liu N, Luo F, Wu H, Liu Y, Zhang C (2008) One-step ionic-liquid-assisted electrochemical synthesis of ionic-liquid-functionalized graphene sheets directly from graphite. *Adv Funct Mater* 18: 1518–1525
77. Kim TY, Lee HW, Kim JE, Suh KS (2010) Synthesis of phase transferable graphene sheets using ionic liquid polymers. *AC Nano* 4:1612–1618

Publisher's note Springer Nature remains neutral with regard to jurisdictional claims in published maps and institutional affiliations.